PSI Center for Accelerator Science and Engineering

EPFL

Intra-Beam Scattering & Microbunching Instability Studies at SwissFEL

EPFL-LPAP Activity Meeting

Roberta Provvedi (PhD student at PSI / EPFL)
PSI Villigen, 18 June 2026

Contents

- Introduction to X-Ray Free Electron Lasers (X-FELs)
- Electron beam quality requirements
- Physics of two collective effects:
  - Intrabeam Scattering (IBS)
  - Microbunching Instability (MBI)
- Experimental studies and simulations of IBS and MBI at SwissFEL
  - Single-stage compression at Aramis (*hard X-ray beamline*)
  - Multi-stage compression at Athos (*soft X-ray beamline*)
- Conclusions and Outlook

X-Ray Free Electron Laser : 4th Generation of light sources

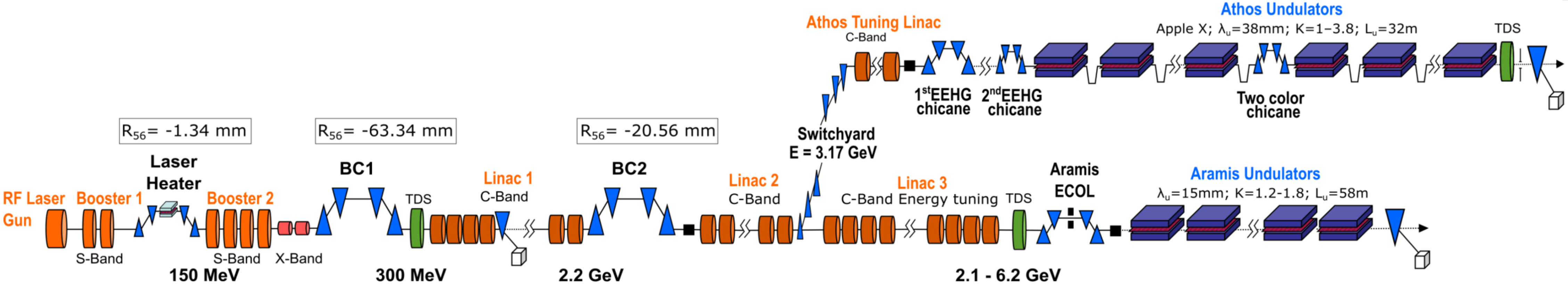

Major technical components

1. RF photo-injector : high-brightness electron beam production
$E_{inj} \sim 7MeV$, $\sigma_\gamma \sim 1 - 2keV$, $\varepsilon_n \sim 150nm$, $I_p \sim 20A$

2. LINACs : boosting the beam energy up to GeVs with RF cavities;

3. Bunch Compressors : increase the peak current and reduce the bunch length (kA bunches with $10s\ fs$). Typically, 2-3 compression stages;

4. Undulator beamline : hosting several undulator modules, each few m long and with undulator period of few cm;

5. Experimental stations : endstations where the ultra-bright, femtoseconds X-ray pulses are delivered for dedicated research purposes.

SwissFEL – Swiss X-ray Free Electron Laser

Source: https://www.psi.ch/it/swissfel

X-Ray Free Electron Laser : 4th Generation of light sources

XFELs

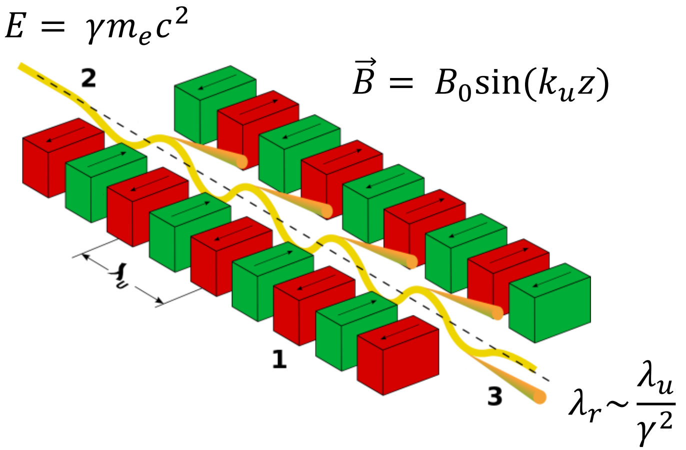

Undulator radiation

- **Central frequency:** $\lambda_r = \frac{\lambda_u}{2\gamma^2}\left(1 + \frac{K^2}{2}\right)$ **Resonance Condition**

  with undulator parameter: $K = \frac{eB\lambda_u}{2\pi m_e c} \sim 1 - 10$

- **Frequency bandwidth:** $\frac{\Delta\omega_r}{\omega_r} \cong \frac{1}{N_u}$

- **Angular spread:** $\Delta\varphi \cong \frac{1}{\gamma\sqrt{N_u}}$

Some properties of X-FEL radiation

- Radiation emitted in undulators has higher power and better quality than the radiation emitted in an individual bending magnet;
- Tunability of the emitted radiation;
- Higher peak brilliance, pulse energies and a better time resolution suitable to study the dynamics of processes occurring at the atomic level;

What makes FELs different from other light sources such as synchrotrons (e.g., SLS at PSI) ?

X-Ray Free Electron Laser : 4th Generation of light sources

FEL instability process

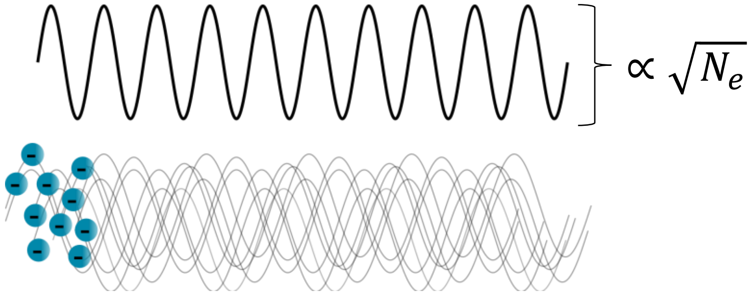

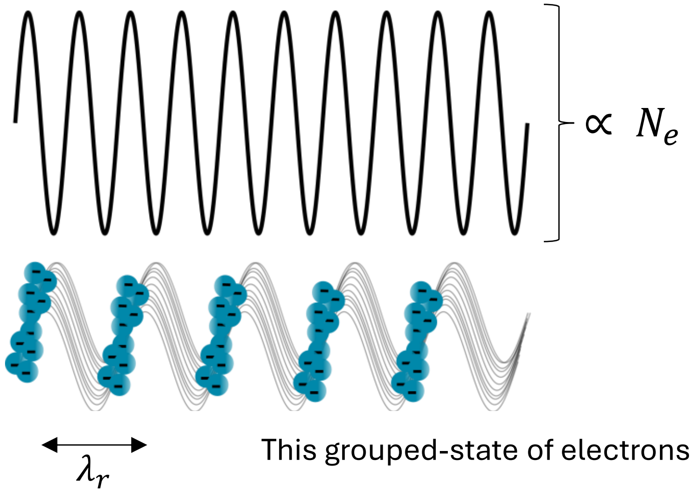

- The bunches longitudinally group together.
- **Microbunching** has periodicity of the FEL wavelength λ_r.
- Bunched beams emit **coherent** FEL radiation, thanks to **constructive interference.**
- **Power scales** $\propto N_e^2$

This grouped-state of electrons is called **'bunching'.**

SASE – Self-Amplified Spontaneous Emission

Initial wave generated by shot noise in the electron bunch. The emission is broadband.

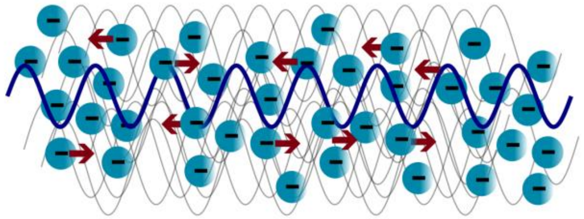

- Transversely coherent
- Longitudinally incoherent

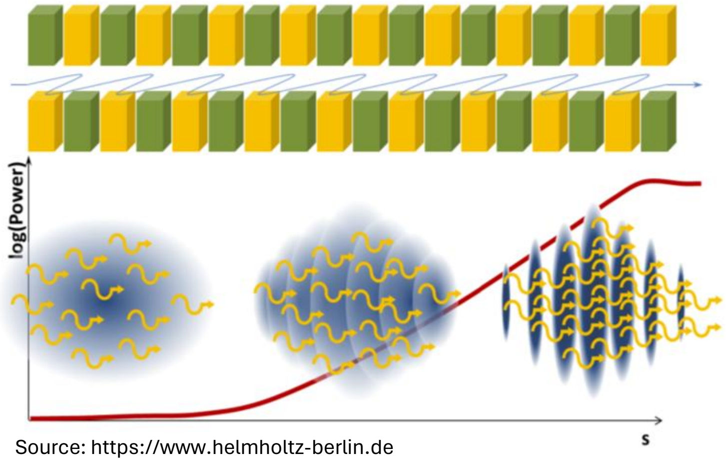

Source: https://www.helmholtz-berlin.de

X-Ray Free Electron Laser : 4th Generation of light sources

FEL instability process

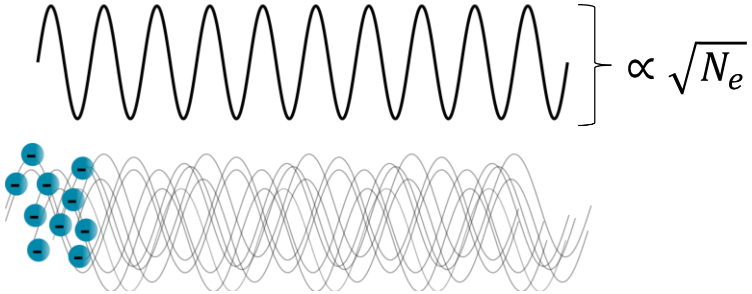

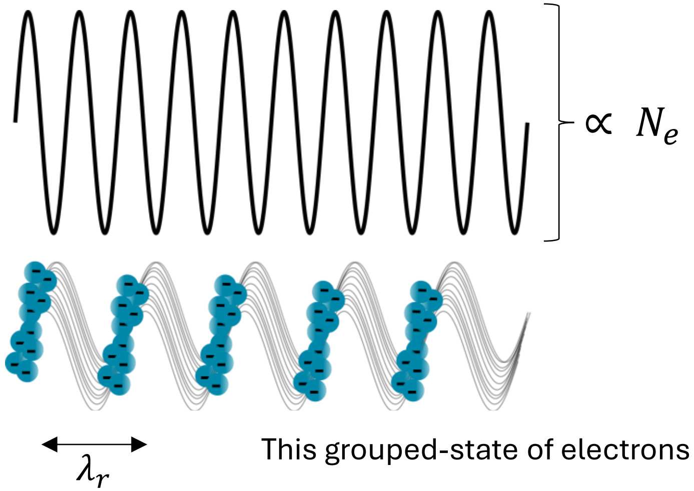

- The bunches longitudinally group together
- **Microbunching** has periodicity of the FEL wavelength λ_r.
- Bunched beams emit **coherent** FEL radiation, thanks to **constructive interference.**
- **Power scales** $\propto N_e^2$

This grouped-state of electrons is called **'bunching'.**

Advanced Seeded-FEL Modes

A seed is used as input signal. The output resembles the seed's characteristics.
E.g., *External seeding (HGHG, EEHG)* – an external laser is used to modulate the beam in energy. The energy modulation scales as and the slice energy spread seen by the FEL process σ_δ :

$$A = \frac{\Delta E}{\sigma_{\delta,int}}$$

- *HGHG* **-** High Gain Harmonic Generation $$\sigma_\delta = \sigma_{\delta,int}\sqrt{1 + \frac{1}{2}A^2}$$
- *EEHG* **-** Echo-Enabled Harmonic Generation $$\sigma_\delta = \sigma_{\delta,int}\sqrt{1 + \frac{1}{2}[A_1^2 + A_2^2]}$$

For good performance seeded FELs need low intrinsic energy spread.

Electron Beam Requirements

PSI

Beam Quality

X-FEL performance is critically determined by the electron beam quality:

$$\rho = \frac{1}{\gamma}\left[\left(\frac{f_c K}{4k_u\sigma_x}\right)^2 \frac{I}{2I_A}\right]^{1/3}$$

Pierce parameter

$$L_g = \frac{\sqrt{3}}{2}\frac{\lambda_u}{4\pi\cdot\rho}\left[1 + \left(\frac{\sigma_\gamma}{\rho\gamma}\right)^2\right]$$

FEL Gain length

$$\frac{\varepsilon_n}{\gamma} \leq \frac{\lambda}{4\pi}, \quad \boxed{\frac{\sigma_\gamma}{\gamma} \ll \rho}$$

Efficiency constraints

$$\mathcal{B}_{6D} = \frac{Q}{\varepsilon_{n,x}\varepsilon_{n,y}\varepsilon_{n,s}}$$

6D beam brightness

λ_u: undulator period
K: undulator parameter
f_c: coupling factor
k_u: undulator wavenumber
σ_γ: beam energy spread
I_A: Alfvén current

- High energies ($\sim GeV$)
- High peak currents (at the keV level for $10s\ fs$ bunch durations)
- Small transverse beam sizes ($10s\ of\ \mu m$)
- Low slice energy spreads ($10^{-3} - 10^{-4}$)
- Low emittances ($< 1\ \mu m$)

To achieve full coherence control, the **electron beam quality** (i.e., intrinsic energy spread, uniformity in beam current and energy across the electron bunch) has significant impact on the FEL parameters and must be optimized.

Collective effects

Non-linear processes degrade the beam quality, i.e., in terms of energy spread and beam brightness, limiting the FEL performance. At SwissFEL, the two main mechanisms, driving the energy spread growth along the accelerator lattice are:

- **Intra-beam scattering (IBS)** - *incoherent single-particle effect*
- **Microbunching instability (MBI)** - *collective dynamics*

Multi-Stage Compression

PSI

Bunch compressor (BC)

- **Chirp :** energy slope in the beam to force electrons to travel different paths in bending magnets (chicane);
- **Coherent Synchrotron Radiation (CSR) :** radiation emitted by a bended relativistic beam. It causes energy spread and emittance growth.
- **Microbunching instability (MBI)** enhancement: chicanes convert energy modulations to density modulations.

$$z_{out} \rightarrow z_{in} + R_{56}\delta + T_{566}\delta^2 + o(\delta^3)$$

$$\delta = \frac{\Delta\gamma}{\gamma} sin(k_u s) + \frac{\sigma_\gamma}{\gamma} + h \cdot z$$

$$R_{56} \cong -\theta^2\left(\frac{4}{3}L + 2D\right)$$

$$h = \frac{d}{ds}\left(\frac{\delta\gamma}{\gamma}\right)$$

$$C = \frac{1}{1 + h \cdot R_{56}}$$

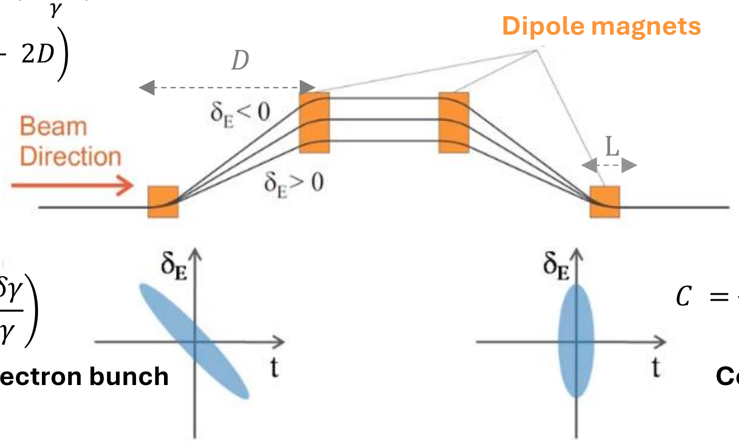

Chirped electron bunch **Compressed bunch**

Multi-stage Bunch Compression

Main advantages :

- Reduction of space charge (SC) effects at low energy
- Mitigation of emittance degradation due to CSR
- Sensitivity to jitter

Main drawback :

- **Microbunching instability growth**

MBI at short wavelength causes **energy spread growth;**

MBI at large wavelengths causes **spectral sidebands excitation**, and bandwidth enlargement of the main seeded line;

⟶ **Understanding MBI dynamics** in high-brightness linacs is needed for optimized operation and future design of longitudinally coherent X-FELS.
⟶ **Optimization of multistage bunch compression** is essential to avoid tight RF tolerances and severe bunch distortions due to MBI.

Microbunching Instability (MBI)

- Microbunching Instability (MBI) is the most relevant **collective dynamics** whenever a high-brightness electron beam experiences acceleration, focusing/defocusing, and bunch compression.

- In the transport sections, upstream of the undulators, the most relevant **collective mechanisms** are:
  - **Longitudinal Space Charge (LSC)** — Drifts sections
  - **Coherent Synchrotron Radiation (CSR)** — Dispersive sections

- E.g., **microbunched beam** measured at the Athos Beam Dump (visible degradation of the longitudinal beam quality)

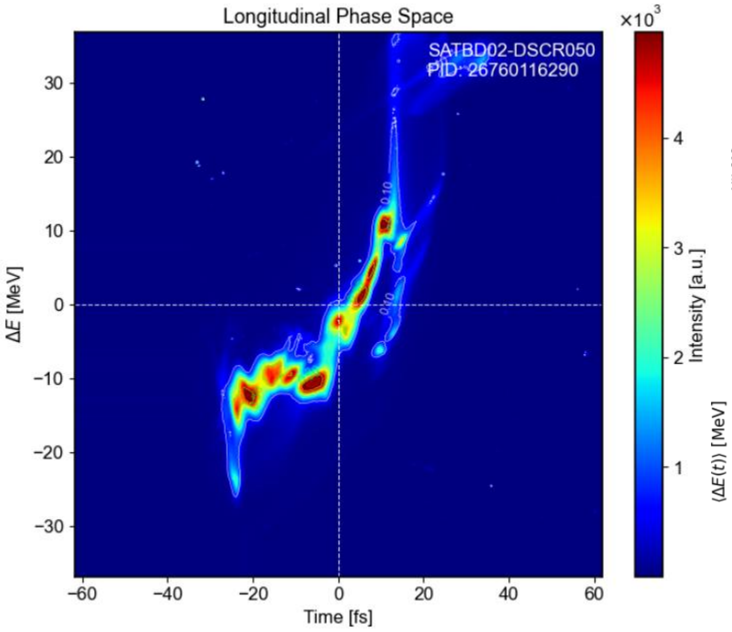

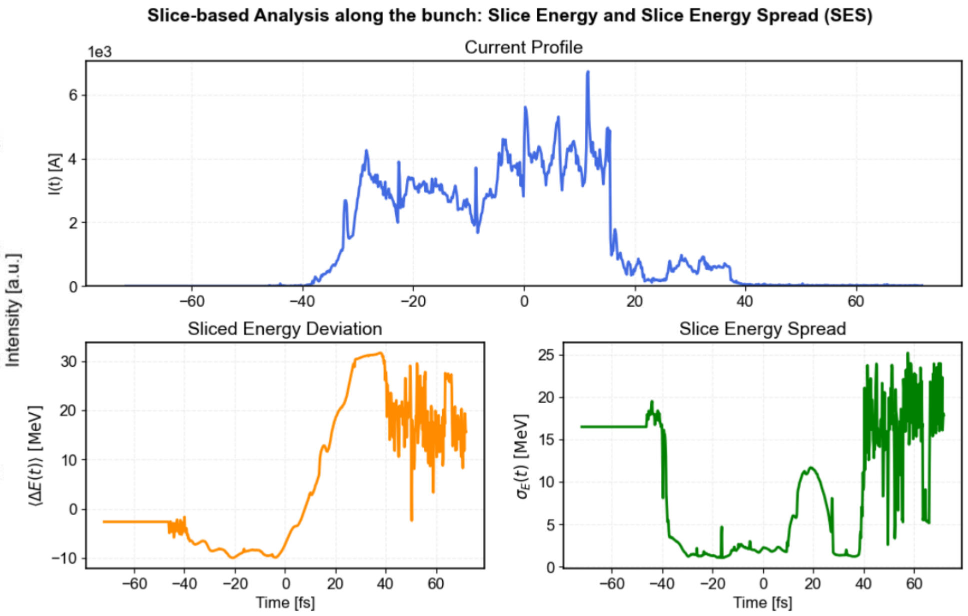

Pulse: 26760116290
Dominant MBI modulation : λ = 2.61 μm
Dominant MBI-Amplitude : A = 20.91

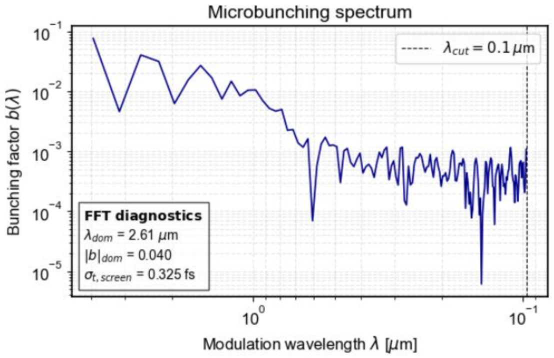

Microbunching Instability (MBI)

MBI

Microbunching instability is **spurious harmonic content** in the longitudinal phase space (LPS) of high brightness electron beams.

- Originated from shot noise, photocathode non-uniformities
- Modulation wavelengths in the range $1 - 100s\ \mu m$

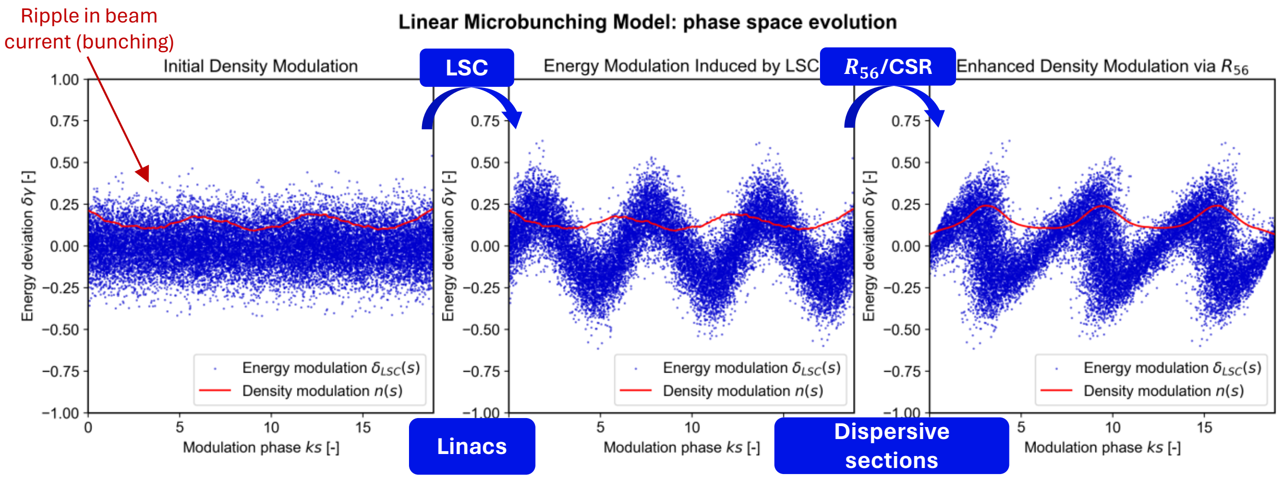

Bunching factor

$$b(k;s) = \frac{1}{Nec}\int I(z)\, e^{-ikz} dz$$

MBI-induced energy modulation
energy dependent, s-integral

$$\Delta\gamma(k;s) = -\frac{4\pi I}{I_A} b(k) \int_0^{\tau} \frac{Z(k;\tau)}{Z_0}\, d\tau$$

ELEGANT Simulation – LPS evolution along the lattice

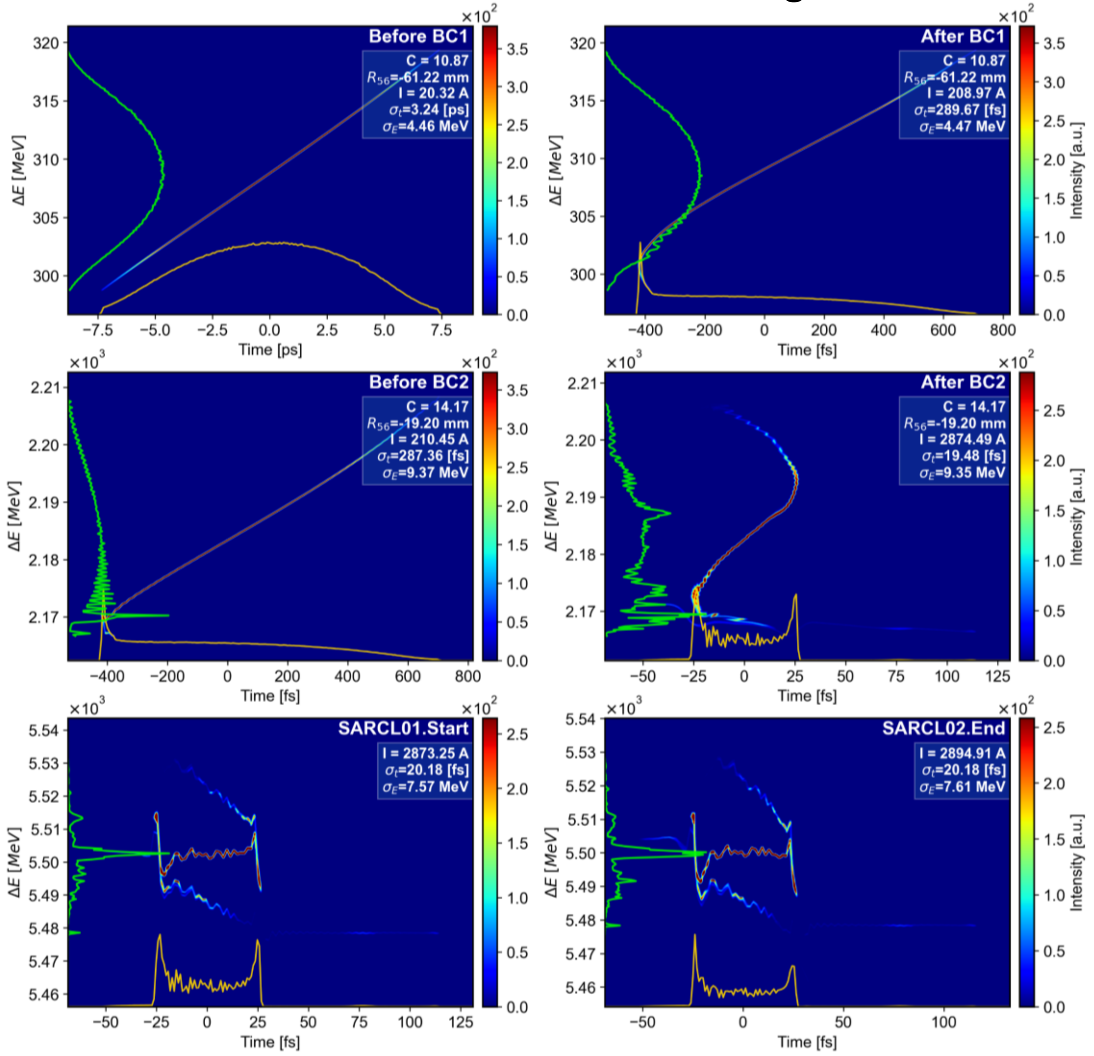

Modelling MBI

How is MBI treated analytically?

Huang-Kim (HK) formalism

Linearization of the Vlasov-Maxwell equation in integral form, for electron beam distribution passing through a four-dipole symmetric chicane. Physics of collective effects (LSC, CSR) is included through frequency dependent effective impedances.

$$b[k(s);s] = b_0[k(s);s] + \int_0^s d\tau K(\tau,s) b[k(\tau);\tau]$$

$$K(\tau,s) = ik(s)R_{56}(\tau \to s)\frac{I(\tau)Z[k(\tau);\tau]}{\gamma I_A}\mathcal{L}_{damping}$$

Bosh-Kleman (BK) formalism

Model based on matrix formalism for longitudinal modulations in the 2D longitudinal phase space. Low gain terms included. Collective effects included: LSC, CSR, CER.

$$T_{ij} = M_{ia}^{(n)} M_{ib}^{(n-1)} \dots M_{zj}^{(1)}$$

$$\begin{pmatrix} b(k,s_1) \\ p(k,s_1) \end{pmatrix} = \begin{pmatrix} T_{11} & T_{12} \\ T_{21} & T_{22} \end{pmatrix} \begin{pmatrix} b(k,s_0) \\ p(k,s_0) \end{pmatrix}$$

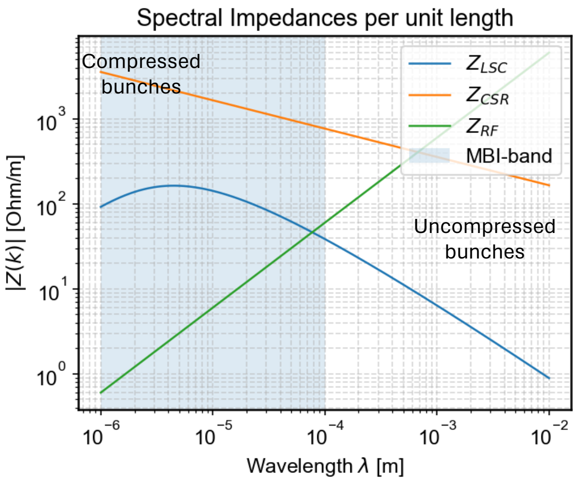

Frequency-dependent effective impedances:

- Longitudinal Space Charge (LSC): $Z_{LSC}(k;s) = i\frac{Z_0}{\pi k r_b{}^2}[1 - 2I_1(\xi)K_1(\xi)], \xi = \frac{k \cdot r_b}{\gamma(s)}, r_b = 0.8735(\sigma_x + \sigma_y)$
- Coherent Synchrotron Radiation (CSR): $Z_{CSR}(k) = \frac{Z_0\, k^{1/3}}{\pi R^{2/3}}(0.41 + i\, 0.23)$ R : dipole bending radius
- Geometric longitudinal impedance of the RF structures: $Z_{RF}(k) \approx i\frac{Z_0}{\pi k a^2}$ a : inner iris radius of the RF structure

MBI Spectral Gain – High Gain Approximation

MBI

Main indicators of MBI strength:

MBI-Gain (RF accelerating structures + chicane) :

$$G(k_u;s) = \left|\frac{b_f(k_d;s)}{b_i(k_u;s)}\right| \simeq C k_u |R_{56}| \underbrace{\frac{4\pi}{Z_0}\frac{I_0}{I_A}\left|\int_0^s \frac{Z_{LSC}(k_u;\tau)}{\gamma(\tau)} d\tau\right|}_{\Delta\gamma/\gamma} LD_{\parallel}\, LD_{\perp}$$

– Longitudinal Landau Damping
– Transverse Landau Damping

MBI-induced energy spread:

$$\sigma^2_{E,\mathrm{MBI}}(s) \simeq \frac{(m_E c^2)}{2\pi n_z}\int_{-\infty}^{+\infty} \left|G(k_u;s)^2 \Delta\gamma_f(k_u;s)^2\right| dk_u$$

Assumption: final energy modulations entirely converted into uncorrelated energy spread

- Linear compression factor: $C = (1 + hR_{56})^{-1}$
- Uncorrelated initial energy spread: $\sigma_{\delta,0}$
- Downstream wavenumber (compressed): $k_d = C\, k_u$
- Gain peaked at the wavelength satisfying : $C k_u R_{56} \sigma_{\delta,0} = 1$
- Line charge density: n_z $[m^{-1}]$

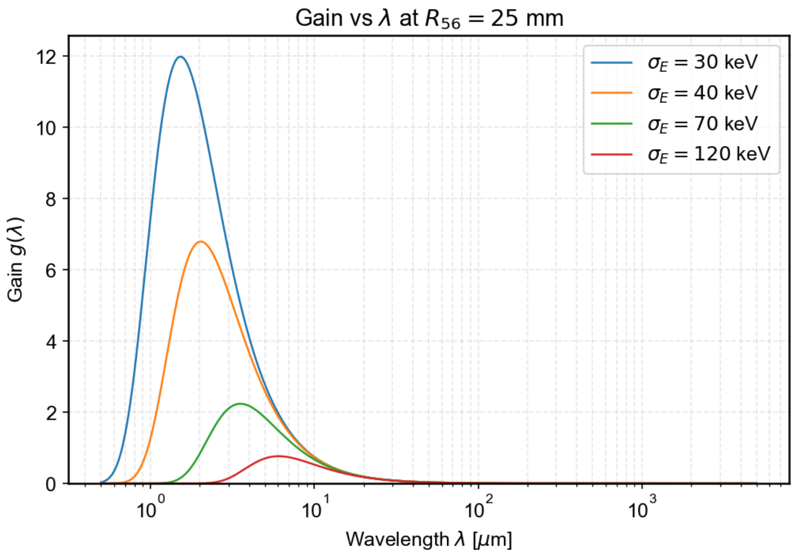

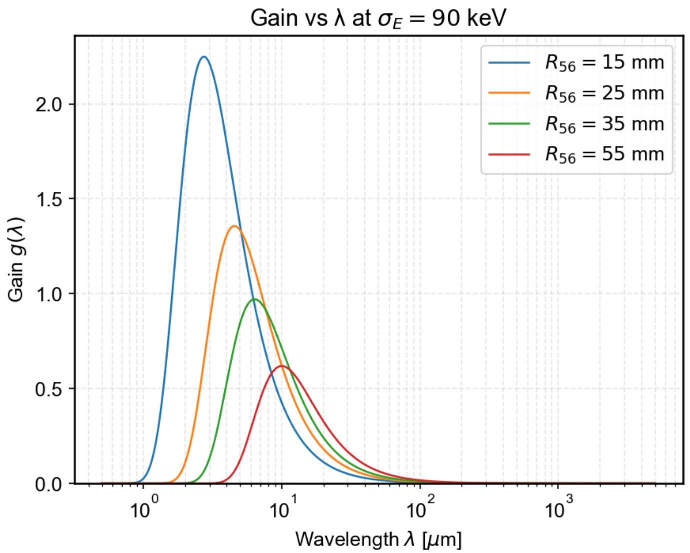

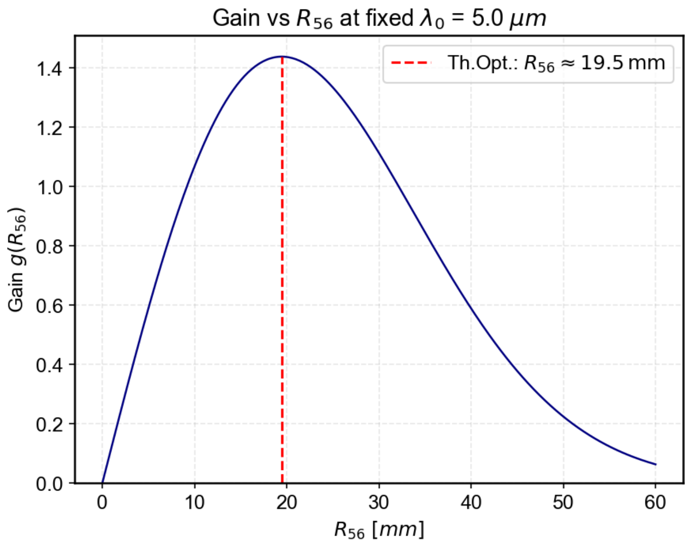

MBI Spectral Gain – High Gain Approximation

PSI

MBI

Two mechanisms for MBI-gain suppression

$$G(k_u;s) = \left|\frac{b_f(k_d;s)}{b_i(k_u;s)}\right| \simeq \frac{4\pi}{Z_0}\frac{I_0}{I_A} C k_u |R_{56}| \left|\int_0^s \frac{Z_{LSC}(k_u;\tau)}{\gamma(\tau)} d\tau\right| exp\left[-\frac{1}{2}\left(Ck_u R_{56}\boldsymbol{\sigma_{\delta,0}}\right)^2\right] exp\left\{-\frac{1}{2}C^2k_u^2\left[\overbrace{\beta_{x0}\left(R_{51} - \frac{\alpha_{x0}}{\beta_{x0}}R_{52}\right)^2 + \frac{R_{52}^2}{\beta_{x0}}}^{\mathcal{H}_x}\right]\varepsilon_{x0}\right\}$$

Amplification term

$LD_{\parallel}$ – Longitudinal or Energy Landau Damping

$LD_{\perp}$ – Transverse or Emittance Landau Damping $k\sqrt{\varepsilon_{x0}\mathcal{H}_x} \geq 1$

$$Z_{LSC}(k_u;\tau) = \frac{Z_0}{\pi k_u {r_b}^2}\left[1 - 2I_1\left(\frac{k\cdot r_b}{\gamma(\tau)}\right)K_1\left(\frac{k\cdot r_b}{\gamma(\tau)}\right)\right]$$

Laser Heater (LH)

In FELs, LSC dominates MBI and the beam initial uncorrelated energy spread is one of the main MBI suppression drivers.

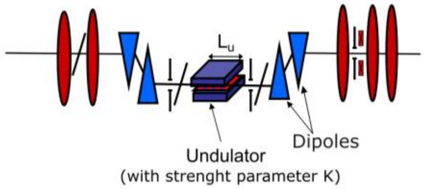

Drawbacks: the LH degrades the beam quality as :

- Energy spread cannot be arbitrarily large;
- Excessive beam heating would also suppress FEL emission;
- Beam transverse emittance grows;

$$\sigma_\delta \approx C\sqrt{\sigma_{\delta,0}^2 + \sigma_{\delta,LH}^2},\ \sigma_{\delta,LH} \cong \frac{L_u}{\sqrt{\sigma_x^2+\sigma_y^2}}\sqrt{\frac{P_L}{2P_0}}\frac{K[JJ]}{\gamma_0^2}$$

- $[JJ] = J_0(\zeta) - J_1(\zeta)$: Bessel functions
- $\zeta = K^2/(4+2K^2)$
- $P_L\ [GW]$: required laser power
- $L_u = N\lambda_u$: undulator length

⟶ *Suppression of MBI at the cost of beam quality degradation (overheating)*

⟶ *It cannot be the definitive solution for stable longitudinal coherence in x-rays production.*

Intra-beam Scattering (IBS)

- **What is IBS?**

  Multiple Coulomb scattering events redistributing particles' momenta from the transverse to the longitudinal degrees of freedom (in XFELs generally: $\sigma_{x',y'} \gg \sigma_\delta/\gamma$), leading to a growth of the uncorrelated energy spread of the electron bunch.

- **IBS Modeling**

  Piwinski's Model [1], modified by Z. Huang [2], slice-dependent by Lucas et al. [3]:

$$\frac{d\sigma_\gamma^2(\mathrm{s})}{dz} = \frac{\sqrt{2\pi} r_e^2 I_p(\mathrm{s})}{4ce\sigma_r(\mathrm{s})\varepsilon_n}\Lambda_\mathrm{c}(\mathrm{s}) \quad \propto I_p\, \gamma^{1/2} \varepsilon_n{}^{-3/2} \beta^{-1/2}$$

  with so-called Coulomb logarithm: $\Lambda_\mathrm{c}(\mathrm{s}) = ln\left(\frac{\Delta\gamma_{max}}{\Delta\gamma_{min}}\right)$, $\Delta\gamma_{max} \approx \gamma^2\sigma_r'$, $\Delta\gamma_{min} \approx \frac{r_e}{\sigma_r\sigma_r'}$, $\sigma_r = \sqrt{\sigma_{x,s}\sigma_{y,s}} = \sqrt{\bar{\beta}(\mathrm{s})\frac{\varepsilon_n}{\gamma(\mathrm{s})}}$

  and locally integrated piecewise: $\sigma_{\gamma,\mathrm{IBS}}^2(s+ds) = \sigma_\gamma^2(s) + \left.\frac{d\sigma_\gamma^2}{dz}\right|_{z=s} ds$ → **Total energy spread**

$$\sigma_{\gamma,\mathrm{tot}}^2 = \sigma_{\delta,0}^2 + \sigma_{\gamma,\mathrm{LH}}^2 + \sigma_{\gamma,\mathrm{IBS}}^2 + \sigma_{\gamma,\mathrm{MBI}}^2$$

- **MBI + IBS Modelling**

  Beam tracking in PELEGANT simulation code + MBI/IBS analytical models, locally evaluated and integrated stepwise along the line:

$$b_{\mathrm{j}+1}(k) = \left[b_\mathrm{j}(k) - J_1\left(iCkR_{56}\frac{\delta\gamma_\mathrm{j}(k)}{\gamma\mathrm{j}}\right)\right] e^{-\frac{1}{2}\left(CkR_{56}\frac{\sigma_\gamma}{\gamma}\right)^2}$$

$$\delta\gamma_{\mathrm{j}+1}(k) = \delta\gamma_\mathrm{j}(k) - \frac{\mathrm{I}}{e\pi\mathrm{I}_A}\frac{Z_j(k)}{Z_0}\Delta s\, b_j(k)$$

$$\Delta s = s_{j+1} - s_j$$

  IBS enhances $LD_\parallel$ resulting in a reduction of the MBI gain peak.

[1] A.Piwinski, *Proc. 9th Int. Conf. On High-Energy Accel.*, pp405-409 (1974)
[2] Z.Huang, *SLAC report*, LCLS-TN-02-8 (2002) [3] T. Lucas et al., *Scientific Reports* 16, 2629 (2026)

MBI and IBS Studies at SwissFEL

PSI

Studies

In the context of MBI and IBS mitigation, we investigated **different bunch compression configurations**:

- ✓ Characterization microbunching instability (MBI) in frequency domain ⟶ MBI Analyzer Tool
- ✓ Single-stage compression at Aramis
- ✓ Multi-stage compression at Athos

Main goals

- ➢ Development of **FFT-based MBI diagnostics;**
- ➢ Characterization of **IBS role in the energy spread growth;**
- ➢ Access to **bunching** and **MBI-induced energy modulation** at the end of the accelerator lattice;
- ➢ **Experimental reduction of the microbunching amplitude**

⟶ Existence of operating conditions where partial suppression of MBI can be achieved by means of *bunching-energy modulation coupling;*

Single-stage Compression Studies

PSI

Beam evolution under reduced MBI effects (IBS-driven)

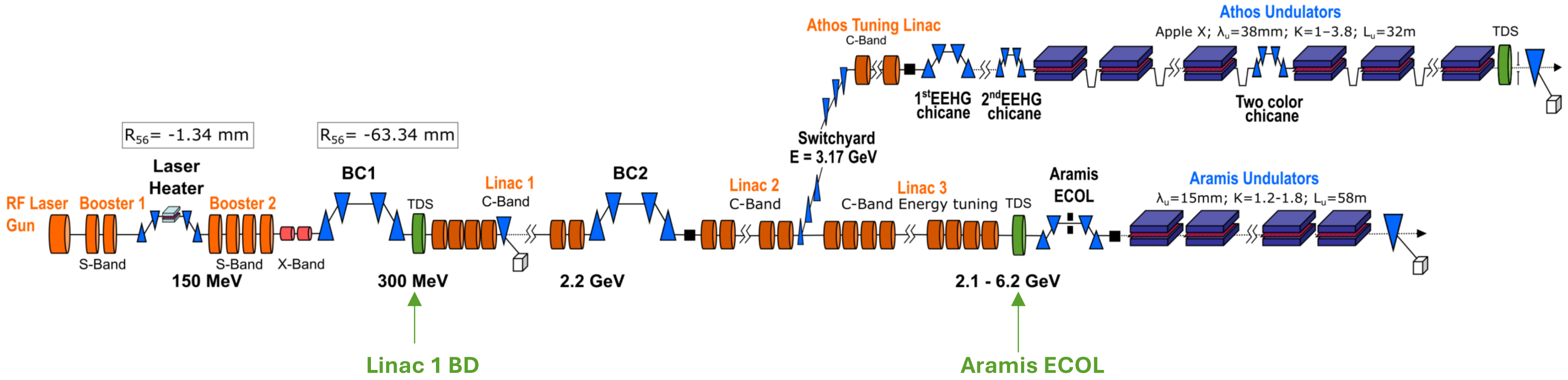

Energy spread studies for $C_2 = 0$ at different peak currents $I_{BC1}[A]$ and locations along the accelerator lattice $z\ [m]$

- **Systematic LPS measurements** in a single-stage bunch compression configuration ($C_2 = 0$), with only **BC1** operated in dispersive mode: | $LH:\ R_{56} = 1.345\ mm$ | $BC1:\ R_{56} = 63.34\ mm$ | $BC2:\ R_{56} = 0.00\ mm$ |
- **Scans:** peak current of the electron beam $I_{BC1}[A]$ scanned from: $95A - 1.4\ kA$ by varying the compression strength in BC1.
- **Slice energy spread (SES) measurements** were performed at a reduced beam energy at the end of Linac 3 (~2.7 GeV) in order to to improve the resolution.
- **TDS diagnostics locations**: downstream of the injector and at the end of Linac 3.

Longitudinal Phase Space (LPS) Diagnostics

Studies

LPS Measurement Method

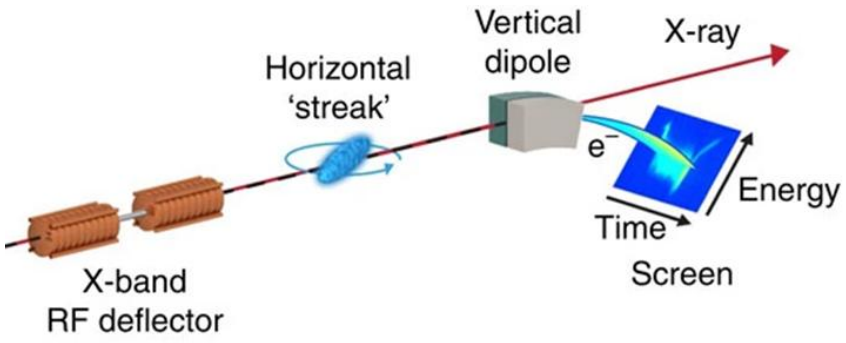

Diagnostic layout: two X-band RF deflecting structures (horizontal streaking) followed by a vertical-bend dipole magnet for measuring the energy spectrum [4].

Radiofrequency (RF) Transverse Deflecting Structure (TDS)

- Time-dependent transverse kick;
- It maps the longitudinal coordinate onto one transverse screen axis;

Two-dimensional profile monitor

- Located in a downstream dispersive section $(\eta \neq 0)$;

LPS calibration

- Temporal coordinate : calibrated using the applied TDS voltage and phase;
- Energy scale: determined from the dispersion at the observation screen;

SwissFEL is equipped with multiple TDS with different frequencies and resolutions:

- **S-band TDS :** 3 GHz, ~1 fs resolution, located in the injector section;
- **C-band TDS:** 5.7 GHz, ~1 fs resolution, located downstream of Linac 3;
- **X-band TDS :** 12 GHz, <1 fs resolution, located at the Athos beam dump.

$$\sigma_y = \sqrt{\eta_y{}^2(\sigma_{\delta,0}{}^2 + \sigma_{TDS}{}^2) + (\beta_y \cdot \varepsilon_y) + \sigma^2{}_{SCR}}$$

[4] Behrens, C., Decker, FJ., Ding, Y. *et al.*, *Nat. Commun.* 5, 3762 (2014).

Single-stage Compression Studies

PSI

Studies

Experimental results & IBS simulations

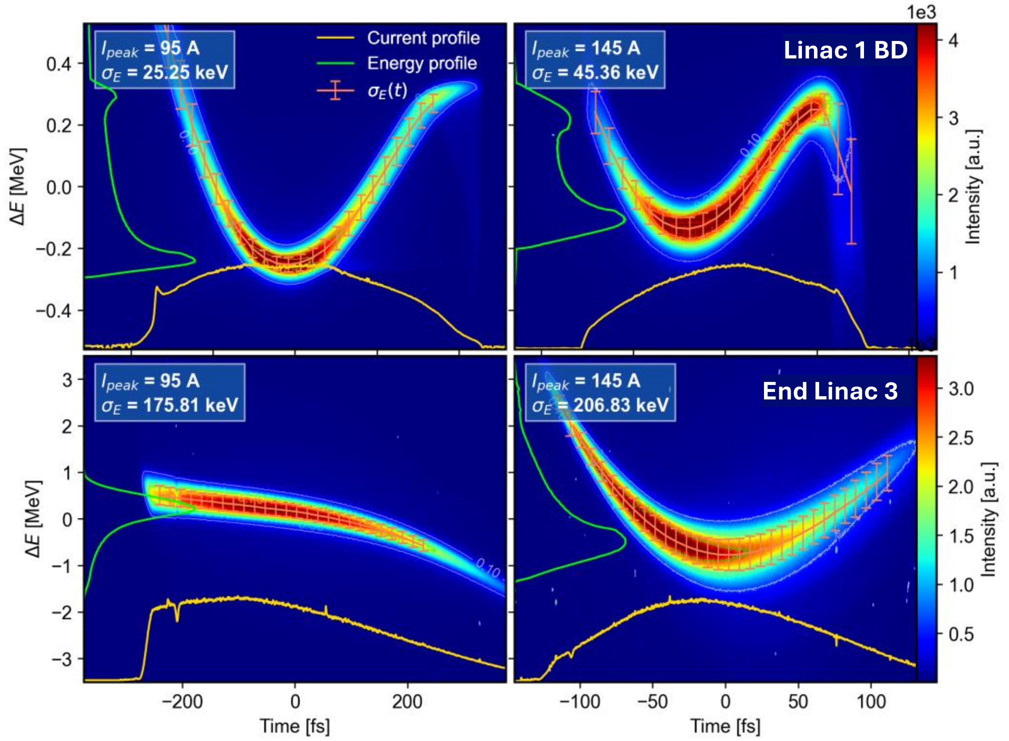

Representative LPS measurements downstream of the injector (top) and at the end of Linac 3 (bottom), at two different peak currents, with associated SES (bunch core).

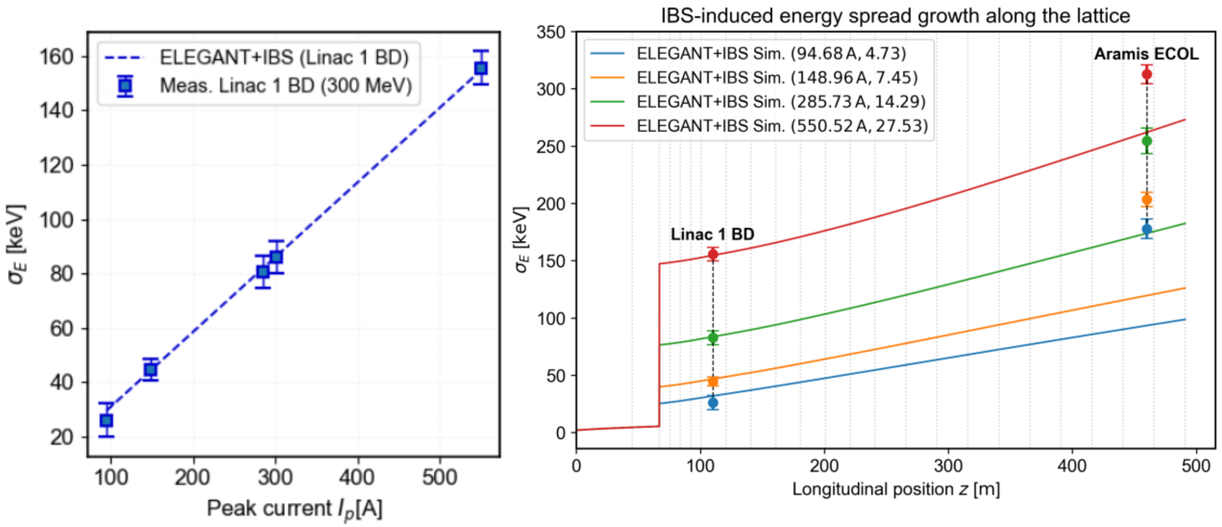

Measured and simulated dependences of the slice energy spread (SES) on the electron beam peak current $I_{BC_1}[A]$ and the longitudinal position. SES is defined as the value at the core of the bunch.

Single-stage Compression Studies

Studies

Observations

- Energy spread growth up to the Linac 1 beam dump (BD) consistent with **compression induced effect and the expected IBS-scaling**, in agreement with previous studies at the SwissFEL injector **(E. Prat)** [5].
- On the other hand, measurements at the end of Linac 3 significantly exceed the IBS scaling, indicating a non-negligible MBI contribution to the beam energy spread, even in single-stage compression, **at frequencies which cannot be resolved by the TDS measurements.**

E.g., Experimental bunching spectrum extracted from measured LPS through 1D FFT on the horizontal projection

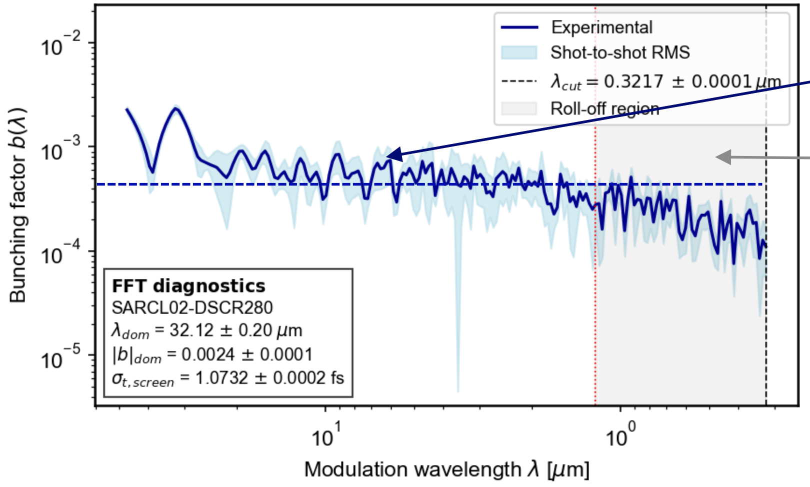

Plateau with overlapped fluctuations – Noise floor:

$$b_{noise} \sim \frac{1}{\sqrt{N_p}}$$

At high-frequencies, decay in the bunching spectrum could be due to either a **TDS-resolution limit** (MBI high-freq. ripples not resolved) or due to **Landau damping suppression of high frequencies**:

$$exp\left[-\frac{1}{2}\left(Ck_u R_{56}\sigma_{\delta,0}\right)^2\right]$$

[5] E. Prat et al., *Phys. Rev. Accel. Beams*, vol. 25, p. 104401, 2022.

Single-stage Compression Studies

Studies

Preliminary simulations IBS&MBI

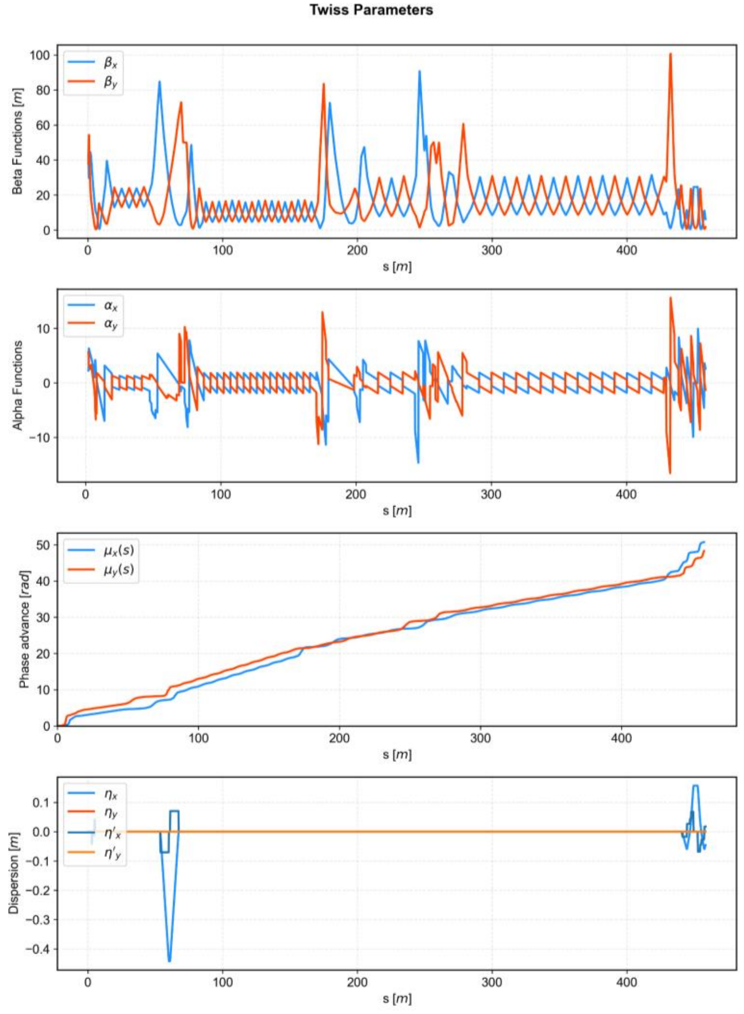

- Number of macroparticles: 1.97E+05
- Peak Current: 91.84 A
- Compression factor (BC1): 4.61

ELEGANT simulation – Single stage compression settings (Case 1°)

Initial Beam Distribution (ASTRA code)

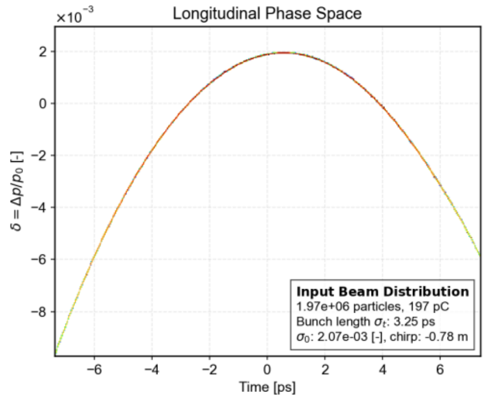

Final LPS Distribution (Aramis ECOL)

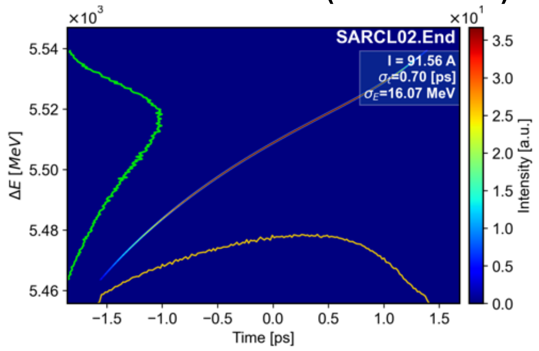

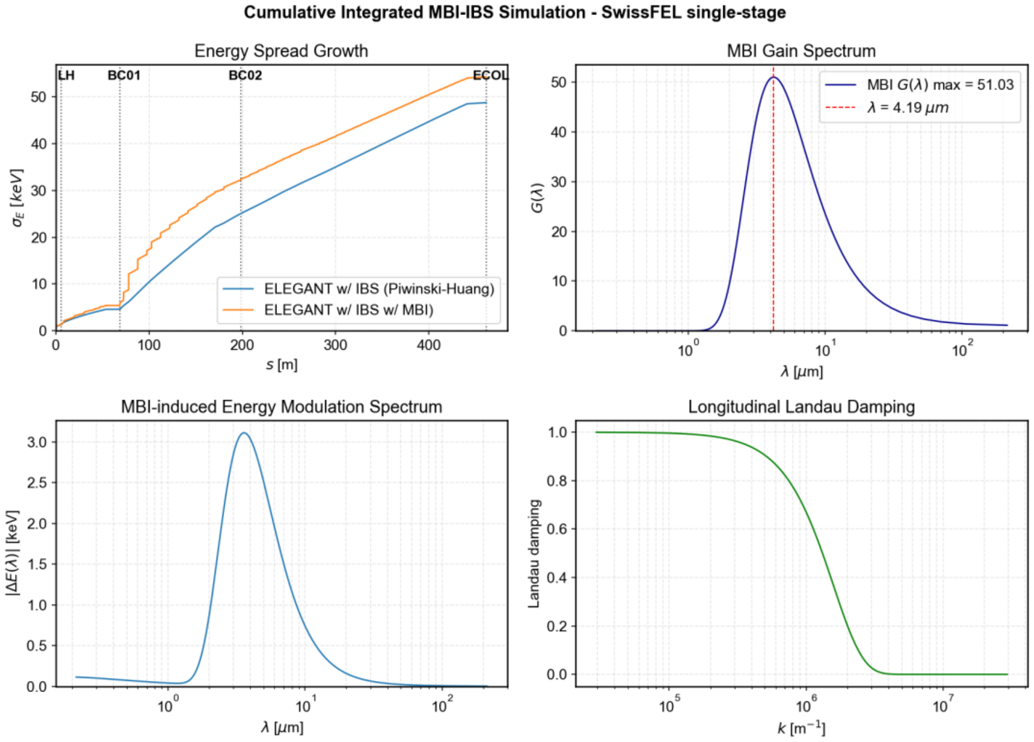

Multi-stage Compression Studies at Athos

Studies

Nominal bunch:

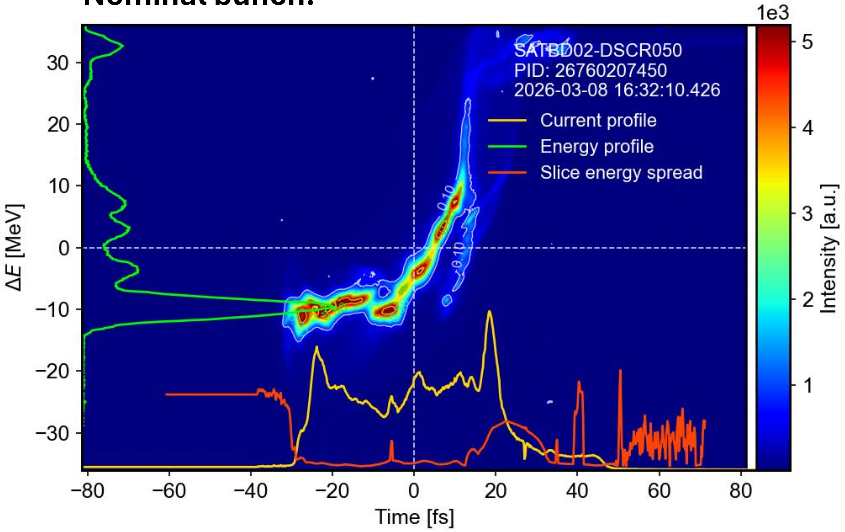

Decompressed bunch:

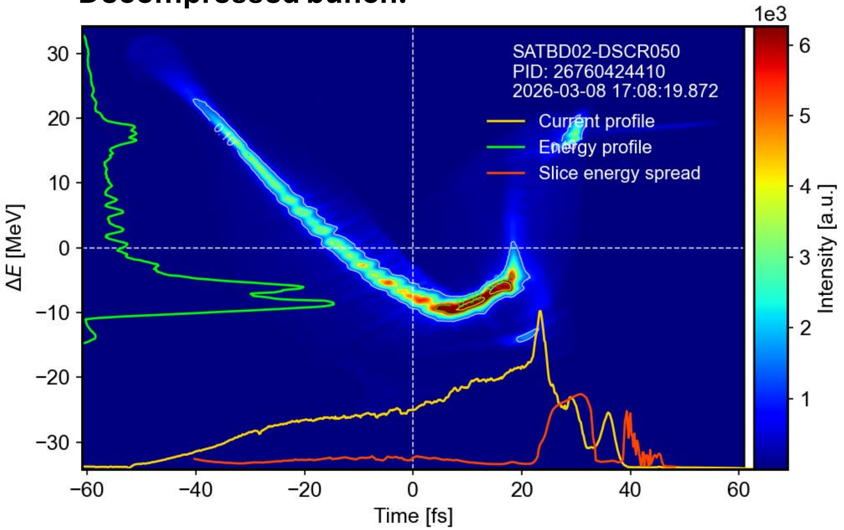

Three/four-stage compression configurations, involving: **BC1 | BC2 | Athos switchyard as a dispersive transport line| EEHG chicane at SATUN05;**

- LPS diagnostics performed at **the Athos beam dump;**
- **Two bunch settings:** nominal bunch $(20.21 \pm 0.70\ fs)$ and a decompressed beam $(45.89 \pm 0.89\ fs)$;
- Dedicated MBI investigation under controlled conditions by scanning the longitudinal dispersion $R_{56}[\mu m]$ at the Athos undulator entrance:

Compression stage	Longitudinal dispersion
BC1	$R_{56} = 63.34\ mm$
BC2	$R_{56} = 20.56\ mm$
EEHG at SATUN05	$R_{56} \approx 0 \div 420\ \mu m$

- Pronounced distortions of LPS and increased SES compared to the single-stage compression ⟶ *High-frequency microstructures consistent with MBI development.*

E.g., in figure are shown measured LPS in a four-stage compression scheme, with EEHG chicane $R_{56} = 104.25\ \mu m$. MBI features:

- Nominal bunch: $\lambda_{MBI} = 1.90 \pm 0.11\ \mu m$ | $A_{MBI} = 15.86 \pm 0.34$
- Decompressed: $\lambda_{MBI} = 0.70 \pm 0.05\ \mu m$ | $A_{MBI} = 8.49 \pm 0.1$

Multi-stage Compression Studies at Athos

Studies

The scanned R_{56} enables controlled LPS manipulation, modifying both the *coupling energy-density modulation* and the *damping of the high-frequency components* through the finite slice energy spread.

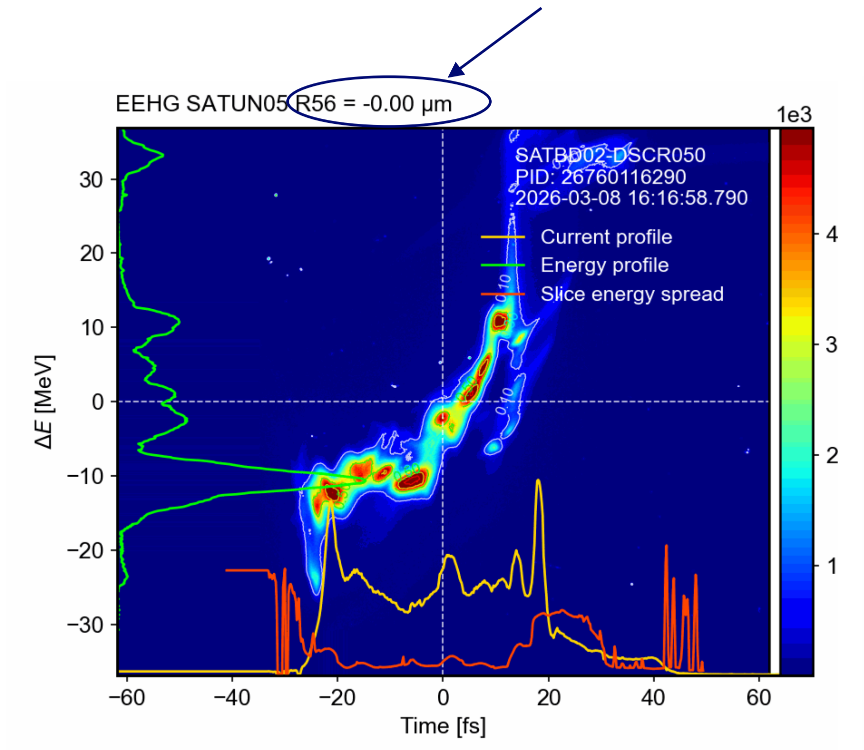

Nominal bunch

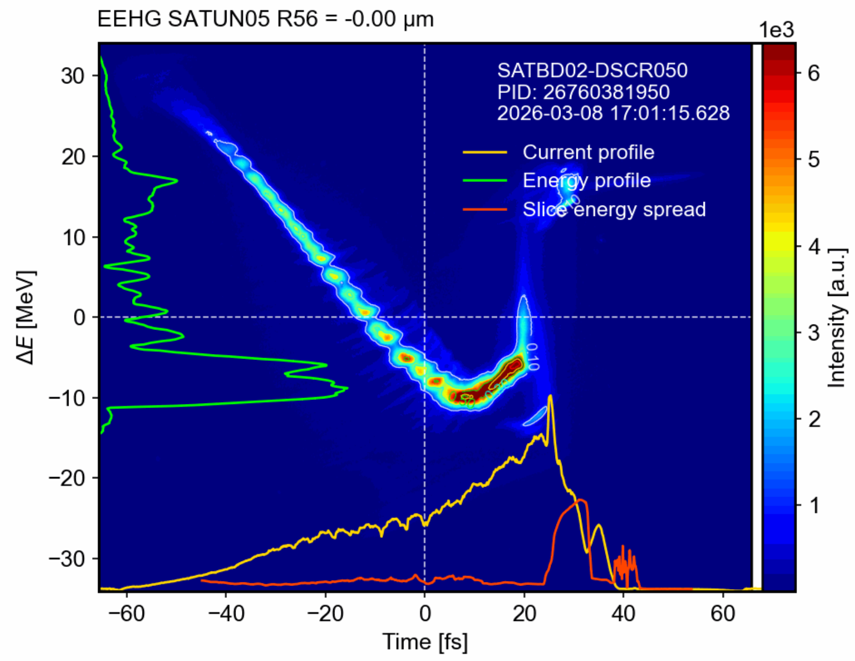

Decompressed bunch

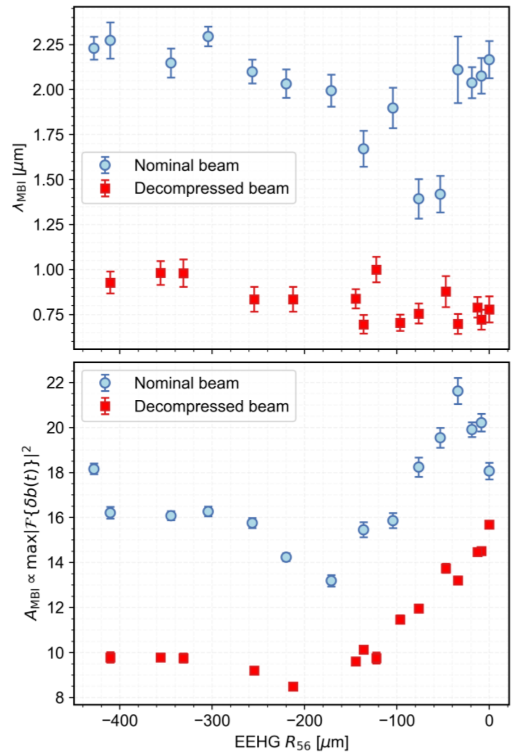

MBI analysis in frequency domain

Microbunching instability (MBI) characterization

Studies

MBI analysis in frequency domain

Beam spectral content in terms of:

- High-frequency microstructures;
- MBI-induced energy modulation $\delta\gamma_i(k)$ *(even if smaller than the uncorrelated energy spread σ_γ);*

Experimental scalar metric of MBI strength:

$$A_{MBI} \equiv \frac{\max[|\mathcal{F}\{\delta b(t)\}|^2]}{\langle|\mathcal{F}\{\delta b(t)\}|^2\rangle} \propto |b(k)|^2$$

with:

- $\mathcal{B}(f) = \mathcal{F}\{\delta b(t)\}$ - *bunching spectrum* i.e., Fourier transform of the density modulations.
- $S_b(f) = |\mathcal{B}(f)|^2 = \left|\int \delta b(t) e^{-i2\pi f t} dt\right|^2$ - *spectral power of the longitudinal density modulations*.

$$b_f(k) = \left[b_i(k) - J_1\left(iCkR_{56}\frac{\delta\gamma_i(k)}{\gamma}\right)\right] e^{-\frac{1}{2}\left(CkR_{56}\frac{\sigma_\gamma}{\gamma}\right)^2}$$

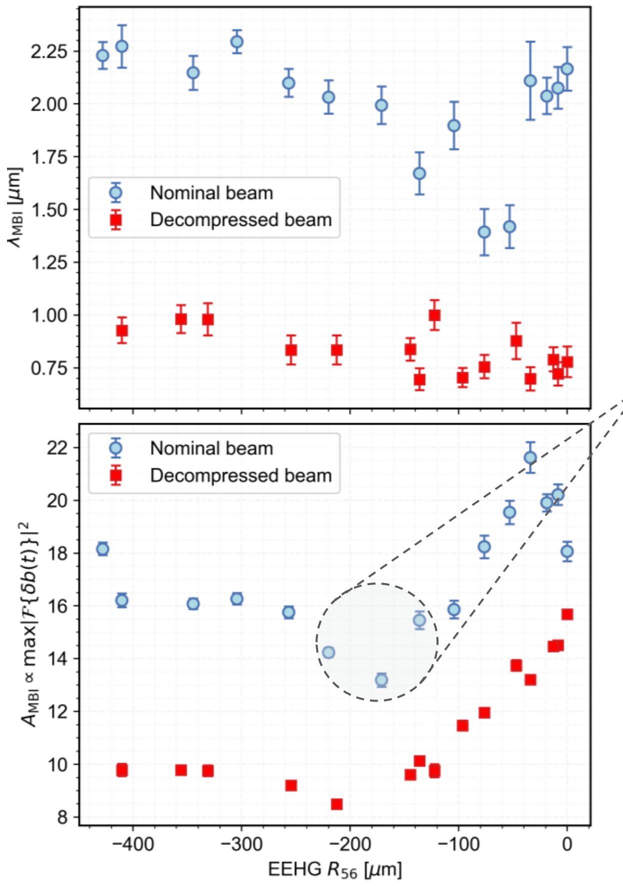

Top: Dominant microbunching wavelength (extracted from 1D temporal FFT of the horizontal projections)

Bottom: Dominant MBI amplitude as a function of the longitudinal dispersion of the EEHG chicane.

Partial suppression of the bunching $b_i(k)$ through its coupling to energy modulation $\delta\gamma_i(k)$, via a tunable small R_{56} $[\mu m]$.

Distinct from longitudinal LD suppression method, this is an MBI mitigation strategy without spoiling the beam.

Decompressed beam: minimum at larger R_{56} (stronger longitudinal dispersion for effective smearing).

Conclusions and Outlook

PSI

Conclusions

- Systematic investigation of IBS- and MBI-driven phase-space evolution at SwissFEL, combining high-resolution LPS diagnostics with frequency domain analysis (FFT) of the microbunching instability;
- Experimental characterization of IBS and MBI features as well as the beam spectral content under different compression schemes;
- Quantified the sensitivity of MBI dynamics to dispersive optics;
- Demonstrated the possibility of **partial MBI suppression** via phase-mixing;

→ This suggests that small dispersive chicanes inserted between compression stages could provide an effective strategy for mitigating MBI instability.

Future Work

- Quantitative benchmarks with MBI semi-analytical models (Huang-Kim formalism) and start-to-end simulations;
- **Optimization of multi-stage compression schemes** for SwissFEL, to mitigate the MBI impact on the FEL spectrum;
- **Multi-bend Athos switchyard** role in MBI amplification + Extension of the analytical MBI model to include it;
- Characterization of **MBI-induced sidebands** around the seeded wavelength which limits the spectral purity.

Thank you for your attention!